Giant titanium electron wave function in gallium oxide: A potential electron-nuclear spin system for quantum information processing

Frédéric Mentink-Vigier,[1] Laurent Binet,[1,*] Gerard Vignoles,[1] Didier Gourier,[1] and Hervé Vezin[2]
[1]*Laboratoire de Chimie de la Matière Condensée, UMR-CNRS 7574, École Nationale Supérieure de Chimie de Paris (Chimie-ParisTech), 11, Rue Pierre et Marie Curie, 75231 Paris Cedex 05, France*
[2]*Laboratoire de Spectrochimie Infrarouge et Raman, UMR-CNRS 8516, Université des Sciences et Technologies de Lille, 59655 Villeneuve d'Ascq Cedex, France*
(Received 17 June 2010; revised manuscript received 13 October 2010; published 11 November 2010)

The hyperfine interactions of the unpaired electron with eight surrounding ^{69}Ga and ^{71}Ga nuclei in Ti-doped β-Ga_2O_3 were analyzed by electron paramagnetic resonance (EPR) and electron-nuclear double resonance (ENDOR) spectroscopies. They are dominated by strong isotropic hyperfine couplings due to a direct Fermi contact interaction with Ga nuclei in octahedral sites of rutile-type chains oriented along **b** axis, revealing a large anisotropic spatial extension of the electron wave function. Titanium in β-Ga_2O_3 is thus best described as a diffuse (Ti^{4+}-e^-) pair rather than as a localized Ti^{3+}. Both electron and ^{69}Ga nuclear spin Rabi oscillations could be observed by pulsed EPR and pulsed ENDOR, respectively. The electron spin decoherence time is about 1 μs (at 4 K) and an upper bound of 520 μs (at 8 K) is estimated for the nuclear decoherence time. Thus, β-Ga_2O_3:Ti appears to be a potential spin-bus system for quantum information processing with a large nuclear spin quantum register.

DOI: 10.1103/PhysRevB.82.184414 PACS number(s): 76.70.Dx, 03.67.Lx, 76.30.Fc

I. INTRODUCTION

NMR has long been recognized as a fruitful approach to quantum information processing (QIP), owing to the very long nuclear spin decoherence times and the easy implementation of unitary transformations and quantum gates with radio-frequency pulses. However, further developments are severely limited by the weak thermal nuclear spin polarizations achievable in the liquid state resulting in highly mixed quantum states and separable density matrices.[1,2] Therefore the approach to NMR-based QIP has shifted to the solid state, where higher polarizations should be achievable by cooling, optical pumping, or dynamic nuclear polarization (DNP). In this context, Mehring and Jende introduced the concept of spin-bus whereby a set of nuclear spins is monitored by an electron spin.[3,4] This scheme would benefit from the high ratio of electron to nuclear gyromagnetic moments, which should strongly enhance the purity of the nuclear density matrix and the detection sensitivity. However, apart from the initial system CaF_2:Ce^{3+} investigated by Mehring and Jende, no other experimental proposal of spin bus has been considered. Good candidates for spin-bus systems are paramagnetic ions in matrices containing nonzero nuclear spins with strong hyperfine interactions between the central electron spin and the surrounding nuclei to ensure well-resolved hyperfine levels and numerous potential qubits. In this paper we show that Ti^{3+} in gallium oxide β-Ga_2O_3 meets these criteria and may be an interesting potential spin bus. In this system, the spin bus is made of the unpaired electron trapped on titanium (formal electron configuration $3d^1$ for Ti^{3+}) and the nuclear spins of the neighboring ^{69}Ga (I=3/2, abundance 60.1%) and ^{71}Ga (I=3/2, abundance 39.9%). More specifically, we show that strong interactions between the unpaired electron of titanium with at least eight surrounding Ga nuclei result from an anisotropic extension of the electron wave function along the **b** axis. In addition, undoped β-Ga_2O_3, when slightly oxygen deficient, is an n-type semiconductor and is known to exhibit a strong bistable DNP by the Overhauser effect.[5–7] This DNP results in nuclear spin polarizations $\approx 5\times 10^{-3}$ corresponding to spin temperatures $\approx$0.1 K while the environment is at room temperature.[6] This opens the way to schemes combining in a same material a spin-bus and a nuclear spin polarization enhanced by DNP. In this work we focus on the spin-bus part of such schemes through the characterization of the hyperfine interactions between Ti unpaired electron and Ga nuclei by continuous-wave (cw) electron-nuclear double resonance (ENDOR) and a preliminary study of the electron and nuclear spin dynamics by pulsed electron paramagnetic resonance (EPR) and pulsed ENDOR.

II. EXPERIMENTAL

Single crystals of β-Ga_2O_3 doped with TiO_2 were grown by the floating-zone method.[8] The crystals obtained are transparent and slightly red with a ratio $Ti/Ga \simeq 0.003$ (value obtained by inductively coupled plasma/mass spectroscopy analysis performed at Service Central d'Analyze du CNRS, Solaize, France). The UV-visible absorption spectrum shows a broad band at about 518 nm, consistent with a Ti^{3+} in an octahedral site. The crystals have been studied by cw-EPR and cw-ENDOR spectroscopies at 20 K with an X-band (9.4 GHz) Bruker Elexsys E500 spectrometer and by pulsed EPR at 4 K and ENDOR at 8 K with an X-band Bruker Elexsys E580 spectrometer.

The crystal structure of β-Ga_2O_3 (space group C_2/m) is made of twined chains of octahedrally coordinated Ga surrounded by chains of tetrahedral Ga. These chains run along the $C_2 \equiv \mathbf{b}$ axis as shown in Fig. 1. All the cations are located in symmetry planes perpendicular to the **b** axis.

III. ENDOR RESULTS

The EPR spectrum of Ti^{3+} in β-Ga_2O_3 is detectable below 150 K and shown in Fig. 1 for the magnetic field orientation

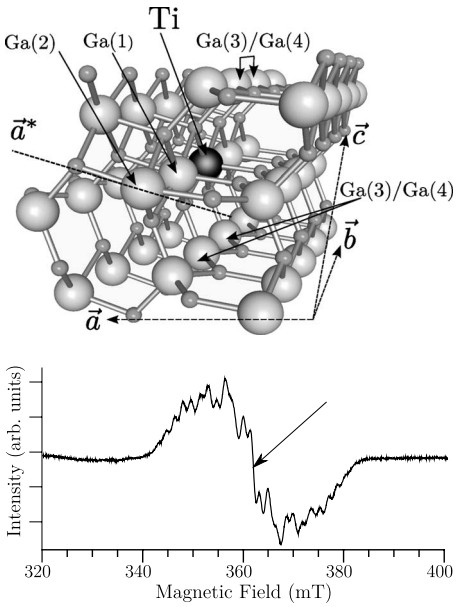

FIG. 1. Top: Crystal structure of β-Ga_2O_3 with a dopant Ti^{3+} in an octahedral site; Ga(1) and Ga(2) are octahedral sites in the same chain as Ti, Ga(3) and Ga(4) are tetrahedral sites nearly related by a reflexion about the $(\mathbf{a}^*,\mathbf{b})$ plane. Small spheres represent oxygen. Bottom: cw-EPR spectrum at 20 K of β-Ga_2O_3:Ti for $\mathbf{b}\|\mathbf{B}_0$. The arrow indicates the field setting for ENDOR experiments.

$\mathbf{B}_0\|\mathbf{b}$. The principal values of the $\hat{g}$ matrix determined from angular variations in the EPR spectrum are $g_x=1.923$, $g_y=1.949$, $g_z=1.850$, with $\mathbf{x}=\mathbf{c}$, $\mathbf{y}=\mathbf{a}^*$, and $\mathbf{z}=\mathbf{b}$. The spectrum exhibits a complex hyperfine structure as shown in Fig. 1 (bottom). Ti possesses only weakly abundant isotopes with nonzero nuclear spins ^{47}Ti ($I=5/2$, 7.4% natural abundance) and ^{49}Ti ($I=7/2$, 5.4% natural abundance). Therefore the EPR spectrum structure cannot arise from coupling with the central Ti nucleus but from couplings with surrounding $^{69/71}$Ga nuclei. However these hyperfine interactions are too complex and largely unresolved with EPR.

ENDOR has the advantage of a much lower spectral density, thus allowing the detection and the identification of each nucleus interacting with the electron spin. Figure 2 (left) represents a cw-ENDOR spectrum recorded at 20 K with a magnetic field setting in the middle of the EPR spectrum [arrow in Fig. 1 (bottom)] and in the $(\mathbf{a}^*,\mathbf{c})$ plane of the crystal. The spectrum contains more than 100 lines and extends over a very large frequency range up to 75 MHz, thus revealing nuclei with very strong hyperfine interactions. Consequently, for each nucleus, we expect two groups of lines centered about $A/2$ and separated by twice the nuclear frequency ν_n (A being the hyperfine coupling). Each of the two groups corresponds to nuclear spin transitions in one of the two manifolds $m_S=\pm 1/2$ of the electron spin. Figure 2 (right) shows an expanded view of the high-frequency part (above 40 MHz) of the cw-ENDOR spectrum, which corresponds to the most strongly coupled nuclei. The angular variations in the positions of the most intense lines for a rotation of the sample about the **b**, $\mathbf{a}^*$, and **c** axes are shown in Fig. 3. First considering only the most intense lines labeled by arrows in Fig. 2 (right) and whose angular variations are shown in the upper part of each diagram in Fig. 3, it can be seen that they consist of four groups of three lines. The topmost two groups are separated by $2\nu_n(^{71}\text{Ga})$ and the down most two groups by $2\nu_n(^{69}\text{Ga})$, where $\nu_n(^{71}\text{Ga})=4.53$ MHz and $\nu_n(^{69}\text{Ga})=3.57$ MHz are the nuclear frequencies of the two isotopes for an external field value $\|\mathbf{B}_0\|=347.9$ mT. These groups of lines are thus unambiguously assigned to Ga nuclei. The splitting of each group into three lines arises from the quadrupolar interaction of these nuclei. Due to their nuclear spin $I=3/2$, three allowed nuclear transitions corresponding to $\Delta m_I=\pm 1$ are expected. The angular dependence of the central lines of these four groups is almost isotropic in any rotation plane (see Fig. 3), indicating a dominantly isotropic coupling via direct Fermi contact interaction. Since these lines correspond to the most strongly coupled Ga nuclei, they can be assigned to the first nearest neighbors, labeled Ga(1) in Fig. 1, located along the **b** axis at 0.304 nm from Ti in octahedral site.

The high-frequency part of the ENDOR spectrum also contains a series of weaker transitions, those unlabeled in Fig. 2 (right). These transitions arise from pairs of magneti-

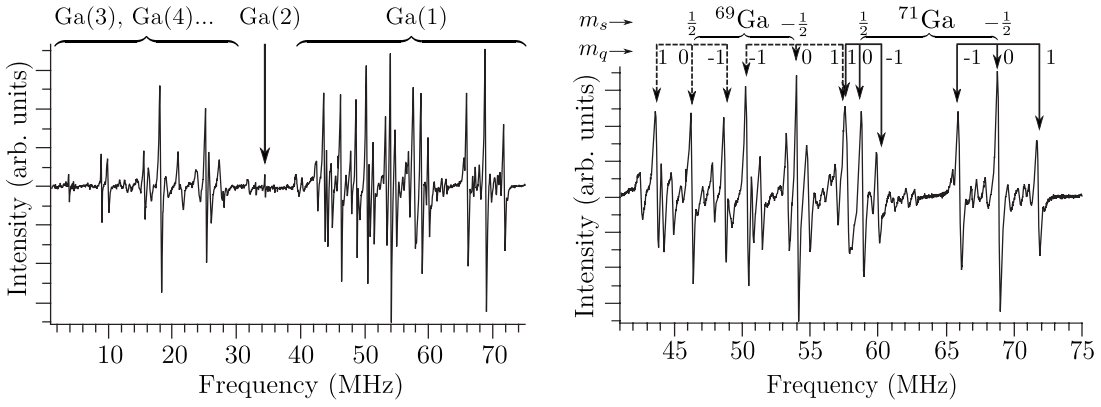

FIG. 2. Left: cw-ENDOR spectrum at 20 K of β-Ga_2O_3:Ti (0.3%) for $\mathbf{B}_0$ in the $(\mathbf{a}^*,\mathbf{c})$ plane with $(\mathbf{c},\mathbf{B}_0)=15°$. Right: Expanded view of the high-frequency part of the ENDOR spectrum. Labeled transitions correspond to Ga(1) nuclei in magnetically nonequivalent pairs ^{69}Ga(1)-Ti-^{71}Ga(1). m_s is the electron spin quantum number and $m_q=\frac{(m_I'+m_I)}{2}$ with m_I and m_I' the nuclear quantum numbers between which a transition takes place. Unlabeled transitions corresponds to pairs of magnetically equivalent isotopes ^{x}Ga(1)-Ti-^{x}Ga(1), $x=71$ or 69 related by the symmetry plane containing Ti and perpendicular to **b**.

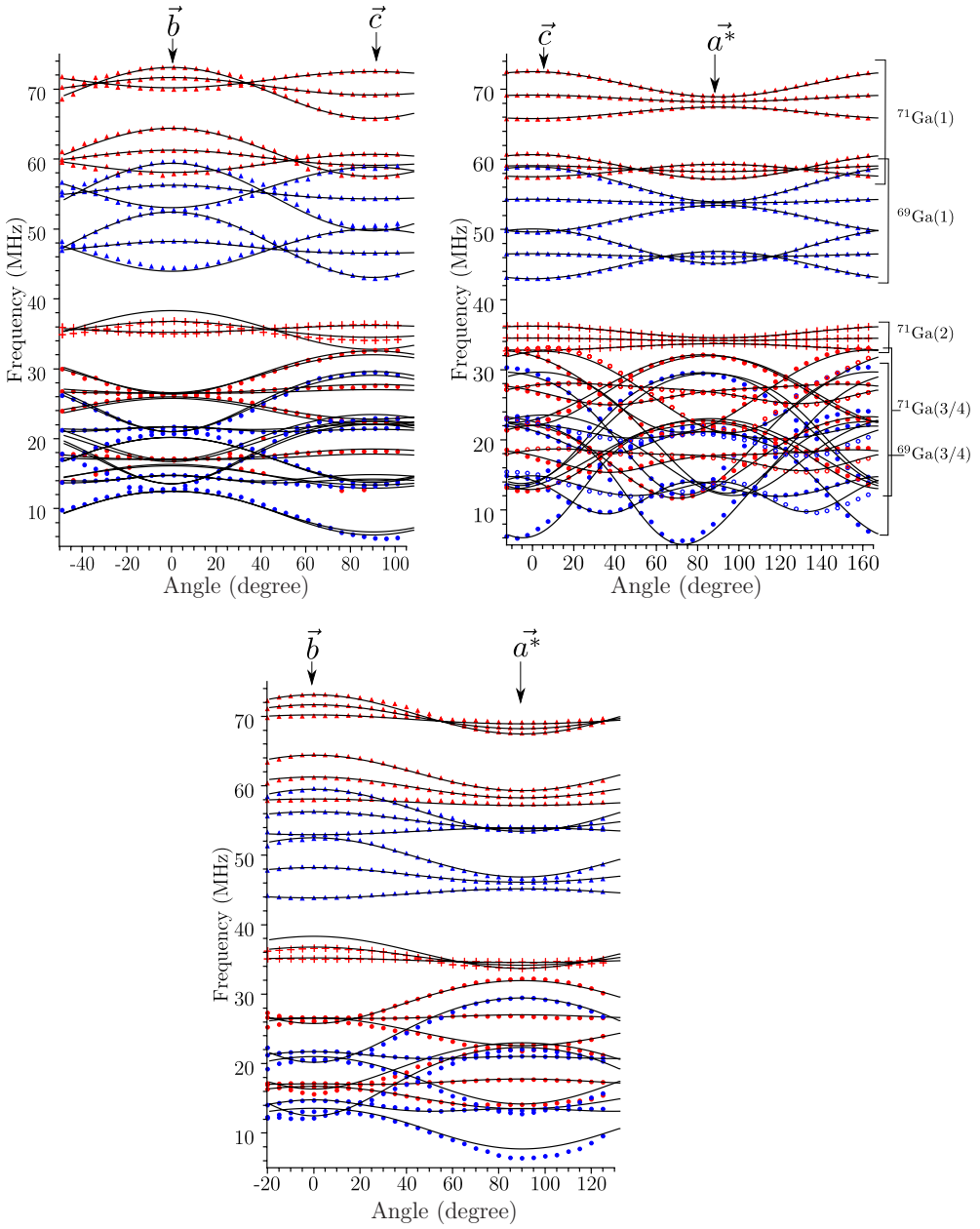

FIG. 3. (Color online) Angular variation in the ENDOR line positions for a rotation about $\mathbf{a}^*$ (top left), **b** (top right), and **c** (bottom). Red (blue) symbols correspond to ^{71}Ga (^{69}Ga), triangles to Ga(1), crosses to Ga(2), empty circles to Ga(3), and filled circles to Ga(4). The full lines are simulations from a second-order perturbation treatment of the spin Hamiltonian with parameters given in Table I.

cally equivalent Ga nuclei: ^{71}Ga(1)-Ti-^{71}Ga(1) and ^{69}Ga(1)-Ti-^{69}Ga(1). In these pairs, Ga nuclei are symmetrical with respect to a plane containing Ti and perpendicular to the **b** axis. In such a pair system, equivalent nuclei are connected by a pseudodipolar interaction leading to additional ENDOR transitions.[9–11] The analysis of the ENDOR of these pairs is beyond the scope of this paper and will be addressed in details in a future work.

In the middle of the ENDOR spectrum, one observes a set of three weak lines centered at about 35 MHz and exhibiting the same angular pattern as ^{71}Ga(1) in the $m_S=-1/2$ manifold. These lines can thus be assigned to ^{71}Ga at the second neighboring position along the **b** axis, labeled Ga(2) in Fig. 1. The ENDOR transitions of ^{71}Ga(2) in the $m_S=+1/2$ manifold and those of ^{69}Ga(2) are presumably too weak to be observed and are lost in the low-frequency part of the spectrum.

The range below 35 MHz in Fig. 3 contains a complex series of angular patterns. A noteworthy fact is that each pattern has an almost symmetrical one with respect to the $\mathbf{a}^*$ axis. These patterns necessarily correspond to pairs of Ga sites, which are approximately related to each other by a reflexion about the $(\mathbf{a}^*,\mathbf{b})$ plane containing Ti. Again, two groups of three lines are expected for each site and each isotope. The closest sites meeting this symmetry requirement are the Ga(3) and Ga(4) sites in Fig. 1, corresponding to the first- and second-nearest tetrahedral Ga at 0.33 nm and 0.344 nm from Ti, respectively. However, these sites are character-

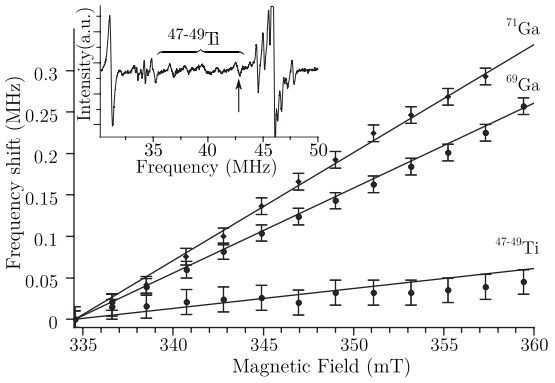

FIG. 4. Absolute frequency shift of the ENDOR lines of ^{71}Ga ($m_s=-1/2, m_q=0$), ^{69}Ga ($m_s=1/2, m_q=0$), and of the line at about 43 MHz for a magnetic field orientation $\mathbf{B}_0 \| \mathbf{a}^*$. Straight lines correspond to theoretical variations in line positions for ^{71}Ga, ^{69}Ga, and $^{47-49}$Ti. The part of the ENDOR spectrum containing $^{47-49}$Ti lines is shown in the inset.

ized by nearly equal hyperfine interactions so that it is impossible to assign each angular pattern either to the Ga(3) site or to the Ga(4) site specifically. Many other transitions are observed in the low-frequency part of the cw-ENDOR spectrum, certainly corresponding to more distant Ga nuclei. However, they are generally too weak to allow a full determination of their rotational patterns, thus forbidding a complete analysis. By simply considering the four identified Ga sites duplicated by the mirror plane, we can calculate that they yield 136 different isotopic Ga configurations and about 10^7 EPR transitions.

Additional weak signals are observed in the 30–45 MHz region of the ENDOR spectrum when $\mathbf{B}_0 \| \mathbf{a}^*$. These signals (see inset of Fig. 4) consist of at least five lines all separated by about 1.2 MHz. This pattern is expected for the two isotopes of Ti which have nonzero nuclear spin, namely, ^{47}Ti and ^{49}Ti with $I=5/2$ and $I=7/2$, respectively. As these two isotopes have almost the same nuclear frequencies ($^{47}\nu_n=0.8654$ MHz and $^{49}\nu_n=0.8657$ MHz at 360 mT) and similar quadrupolar moment ($^{47}Q=0.302$ fm^2 and $^{49}Q=0.247$ fm^2), the lines are expected at almost the same frequencies. In order to identify the nuclei responsible for these weak signals, we studied the variation in the ENDOR line positions with $\|\mathbf{B}_0\|$. Figure 4 represents the shift of the ENDOR line positions against $\|\mathbf{B}_0\|$ for a ^{71}Ga line, a ^{69}Ga line and an unidentified line at about 43 MHz, represented by the arrow in the inset of Fig. 4. Theoretical variations given by $\nu_n=g_n\beta_n\|\mathbf{B}_0\|$ are shown on the figure, with g_n depending on the nucleus, and where second-order hyperfine corrections have been neglected. The $\|\mathbf{B}_0\|$ dependence of the unidentified line is in good agreement with the variation expected for Ti isotopes. However the signal is too weak to be followed in all planes. It decreases rapidly and disappears for $\mathbf{B}_0 \| \mathbf{c}$. We could not obtain the hyperfine tensor for Ti, however the hyperfine interaction for this nucleus is about 50 MHz for the magnetic field orientation $\mathbf{B}_0 \| \mathbf{a}^*$.

IV. STRUCTURE OF THE PARAMAGNETIC CENTER

When several magnetically nonequivalent nuclei interact with the same electron spin, each electron-nucleus pair can be treated as an independent system, described by the following spin Hamiltonian:[10]

$$\mathbf{H} = \beta \mathbf{S} \cdot \mathbf{g} \cdot \mathbf{B}_0 + \mathbf{S} \cdot \mathbf{A} \cdot \mathbf{I} + \mathbf{I} \cdot \mathbf{Q} \cdot \mathbf{I} - g_n \beta_n \mathbf{I} \cdot \mathbf{B}_0, \quad (1)$$

where the terms on the right-hand side are the electron Zeeman, the hyperfine, the nuclear quadrupolar, and nuclear Zeeman interactions, from left to right, respectively. To calculate the corresponding energy levels and nuclear transitions, we used the perturbation treatment up to second order of the Hamiltonian [Eq. (1)] given by equations derived by Iwasaki[12] (see Appendix). The hyperfine and quadrupolar tensors for each identified nucleus were obtained by simulating the angular variations in the positions of the ENDOR lines derived from these equations. Comparison between experimental and calculated angular variations are shown in Fig. 3. The simulations were performed by fitting the spin Hamiltonian parameters. We started the simulation with the high-frequency part of the spectrum corresponding to ^{71}Ga(1) nuclei. The accuracy of the simulation was tested for ^{69}Ga(1) by comparing experimental and theoretical variations calculated with the same spin Hamiltonian parameters scaled to the appropriate g_n and Q parameters for ^{69}Ga. The same procedure was applied to the other ENDOR lines in the order of decreasing frequencies corresponding to ^{71}Ga(2), ^{71}Ga(3/4), and ^{69}Ga(3/4). The spin Hamiltonian parameters are given in Table I for each gallium site, where A_x, A_y, and A_z are the principal values of the hyperfine tensor.

The analysis of the hyperfine interactions, reported in Table II, gives more information about the paramagnetic system. It is decomposed into an isotropic and an anisotropic part $A=A_{\text{iso}}+A_{\text{aniso}}$, with $A_{\text{iso}}=\frac{1}{3}(A_x+A_y+A_z)$ and $A_{\text{aniso}}=\frac{1}{6}(2A_z-A_x-A_y)=A_{\text{dip}}+A_{\text{cov}}$. The dipolar contribution A_{dip} was computed using the point dipole-dipole approximation $A_{\text{dip}}=\frac{g\beta g_n\beta_n}{R^3}$, where R is the distance between Ti and the Ga

TABLE I. Principal values of the hyperfine tensors for the identified ^{71}Ga nuclei and Euler angles (α,β,γ) relative to the (**c**, **a***, and **b**) frame.

Site	Position	Distance Ga-Ti (nm)	A_x (MHz)	A_y (MHz)	A_z (MHz)	(α,β,γ) (deg)
Ga(1)	Octa	0.304	128.1 ± 0.2	126.6 ± 0.5	132.9 ± 0.3	(0,0,0)
Ga(2)	Octa	0.608	59.9 ± 0.2	59 ± 0.5	63.6 ± 0.3	(0,0,0)
Ga(3)	Tetra	0.3301	42.1 ± 0.15	42.7 ± 0.3	47.5 ± 0.15	$(90,90,47\pm4)$
Ga(4)	Tetra	0.3446	42.4 ± 0.15	42.7 ± 0.3	47.6 ± 0.15	$(90,90,-34\pm4)$

TABLE II. Contributions to the hyperfine interactions and spin density ρ_{4s} in the $4s$ orbital for the identified ^{71}Ga sites.

	^{71}Ga(1)	^{71}Ga(3/4)	^{71}Ga(2)
A_{iso} (MHz)	129.2 ± 0.5	44.1 ± 0.3	60.8 ± 0.5
ρ_{4s}	1.67×10^{-2}	5.7×10^{-3}	7.8×10^{-3}
A_{aniso} (MHz)	1.9 ± 0.5	1.7 ± 0.3	1.4 ± 0.5
A_{dip} (MHz)	0.86 ± 0.5	0.63 ± 0.3	0.11 ± 0.5
$A_{cov}=A_\sigma-A_\pi$ (MHz)	1.0 ± 0.5	1.1 ± 0.3	1.3 ± 0.5

nucleus considered. The covalent contribution A_{cov} to the anisotropic interaction is deduced from the experimental value of A_{aniso} and the calculated value of A_{dip}. For each gallium site the hyperfine interaction is dominated by the isotropic interaction A_{iso} (several tens of megahertz) so the main contribution to the hyperfine coupling comes from the Fermi contact interaction, which is the direct delocalization of the unpaired electron onto the $4s$ orbitals of neighboring Ga nuclei. A_{iso} is related to the electron spin density ρ_{4s} in the $4s$ Ga orbital ψ_{4s} by

$$A_{iso} = \frac{2}{3}\mu_0 g_e \beta g_n \beta_n \rho_{4s} |\psi_{4s}(0)|^2 = \rho_{4s} A^0_{iso}, \quad (2)$$

where $A^0_{iso}=7800$ and 6100 MHz (for ^{71}Ga and ^{69}Ga, respectively) is the hyperfine coupling constant for a free Ga^{2+} ion in the ^{2}S spectroscopic state.[13] The values of the electron spin densities ρ_{4s} calculated from Eq. (2) are given in Table II. Considering the twofold multiplicity of each labeled Ga site according to the symmetry $(\mathbf{a}^*,\mathbf{c})$ plane containing Ti, the interactions of the unpaired electron with eight neighboring Ga nuclei have been analyzed: more than 7% of the total electron spin density is delocalized over these nuclei. Interestingly, the spin density is greater on Ga(2) site than on Ga(3)/Ga(4) sites, which are however closer to Ti (0.608 nm versus 0.33/0.34 nm). Assuming an exponential envelope $\psi_{Ti}(r)=A\exp(-r/a)$ for the unpaired electron wave function, the electron spin density is $\rho(r)=|\psi_{Ti}(r)|^2$. From the spin densities in Table II, we may thus estimate a Bohr radius $a \approx 0.8$ nm along **b** much larger than the Bohr radius $a \approx 0.3$ nm in a transverse direction. The unpaired electron wave function thus exhibits a large and anisotropic extension along the **b** axis, corresponding to the direction of octahedral chains (Fig. 1). Therefore, Titanium in β-Ga_2O_3 should be described as a $(Ti^{4+}$-$e^-)$ pair rather than as a Ti^{3+} ion, whereby a conduction electron[6] is trapped by a Ti^{4+} ion in octahedral site. The same trend is observed with the anisotropic part A_{aniso} of the hyperfine coupling. It can be noticed that the covalent contribution $A_{cov}=A_\sigma-A_\pi$ increases with the Ti-Ga distance while the point dipole-dipole interaction A_{dip} decreases. Again, this points out a strong contribution of covalency along octahedral chains, which results from the anisotropic extension of the electron wave function along the **b** axis. Unfortunately, it is not possible to deduce the spin density in $4p_z$ (responsible for A_σ) and $4p_x$, $4p_y$ (responsible for A_π) Ga orbitals since both A_σ and A_π contribute to the covalent part A_{cov} of the hyperfine coupling. It is important to note that the increase in $A_{cov}=A_\sigma-A_\pi$ with the distance R from Ti (see Table II) is not due to an increasing covalency. It only indicates that A_π decreases more rapidly with R than A_σ, which is another indication of the delocalized unpaired electron in $4s$ and $4p_z$ Ga orbitals along octahedral chains.

Complementary information on the paramagnetic center is given by the quadrupolar interaction. The three principal components Q_i $(i=x,y,z)$ of the quadrupolar tensor deduced from ENDOR are given in Table III for the identified Ga nuclei. These values are compared with the values measured in undoped β-Ga_2O_3 crystals by solid-state NMR[14] and by the Overhauser shift of conduction electrons.[15] As usual, the quadrupolar interaction is analyzed in terms of two components $C_q=\frac{eQV_{zz}}{h}=6Q_z$ and the asymmetry factor $\eta=|\frac{Q_{xx}-Q_{yy}}{Q_{zz}}|$, where V_{zz} is the electric field gradient (EFG). The values of C_q and η reported in Table III for an undoped sample are taken from Vosegaard *et al.*[14] From these values, we also calculated the values of Q_i. The values obtained from the Overhauser shift method are almost identical.[15] Comparison of the quadrupolar parameters in β-Ga_2O_3:Ti and in pure β-Ga_2O_3 gives some information about the effect of Ti doping on the asymmetry factor and the EFG seen by neighboring gallium nuclei. Examination of Table III shows that the presence of Ti in an octahedral site does not identically affect the neighboring Ga. Clearly, the quadrupolar interaction in octahedral sites Ga(1) and Ga(2) becomes asymmetrical while the EFG decreases by ≈41% for Ga(1) and ≈59% for Ga(2). On the contrary the effect of titanium doping is very small on neighboring tetrahedral Ga. The asymmetry factor η is not affected within experimental errors, and the EFG seen by Ga(3)/Ga(4) nuclei decreases only by ≈4–5 %. The strong perturbation of neighboring octahedral Ga sites along

TABLE III. Quadrupolar tensors for the identified ^{71}Ga nuclei and Euler angles (α',β',γ') relative to the (**c**, $\mathbf{a}^*$, and **b**) frame.

Sample	Site	Coordination	Q_x (MHz)	Q_y (MHz)	Q_z (MHz)	C_Q (MHz)	η	(α',β',γ') (deg)
Doped	^{71}Ga(1)	Octa	-0.76 ± 0.04	-0.06 ± 0.04	0.82 ± 0.04	4.92 ± 0.24	0.85 ± 0.12	(0,90,0)
	^{71}Ga(2)	Octa	-0.49 ± 0.03	-0.076 ± 0.03	0.57 ± 0.03	3.42 ± 0.18	0.73 ± 0.11	(0,0,0)
	^{71}Ga(3)/	Tetra	-1.69 ± 0.04	-0.11 ± 0.04	1.8 ± 0.04	10.8 ± 0.3	0.88 ± 0.13	$(90,90,101 \pm 1)$
	^{71}Ga(4)	Tetra	-1.65 ± 0.05	-0.11 ± 0.05	1.76 ± 0.05	10.6 ± 0.3	0.88 ± 0.13	$(90,90,90 \pm 1)$
Undoped[a]	^{71}Ga	Octa	-0.7603 ± 0.068	-0.629 ± 0.054	1.390 ± 0.005	8.34 ± 0.03	0.148 ± 0.008	≈(103.7,90,180)
	^{71}Ga	Tetra	-1.721 ± 0.019	-0.1456 ± 0.0016	1.866 ± 0.020	11.20 ± 0.03	0.844 ± 0.007	≈(−4,90,90)

[a]See Ref. 14.

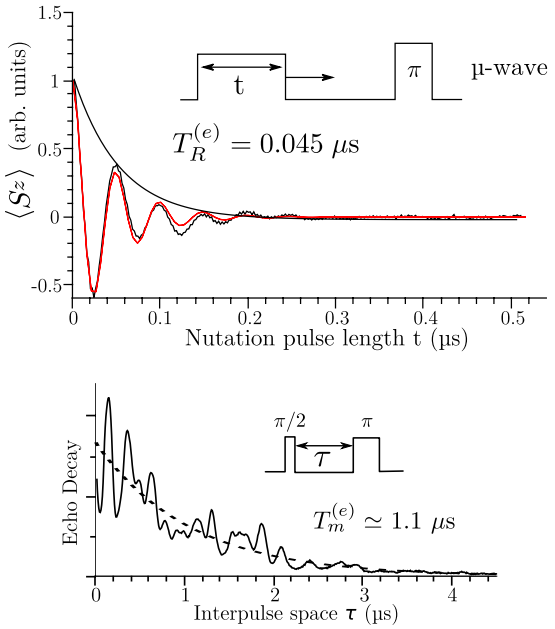

FIG. 5. (Color online) Top: Experimental (black line) and calculated (red line) electronic Rabi oscillations at 4 K for $\mathbf{B}_0 \perp \mathbf{b}$ and $(\mathbf{c},\mathbf{B}_0)=45°$; the nutation experiment is based on a $\pi/2$ pulse of duration 16 ns incremented by a series of 256 pulses of duration 2 ns. The measurement π pulse of duration 28 ns is separated from the nutation pulse by $\tau=220$ ns. The decay of the oscillations according to Eq. (3) is also represented. Bottom: Corresponding electron spin-echo decay recorded with $\pi/2$ and π pulses of duration 16 ns and 32 ns, respectively, and $\tau=200$ ns. The oscillations of the echo decay represent nuclear modulations (electron spin-echo envelope modulation) due to hyperfine interactions with gallium nuclei. The dashed line is a simulation of the background with an exponential decay time $T_m^{(e)}=1.1\ \mu s$.

b axis corroborates the anisotropic electron delocalization on these sites found by analyzing the hyperfine interaction.

V. ELECTRON AND NUCLEAR RABI OSCILLATIONS

The possibility of observing Rabi oscillations[16] in a quantum system is required to construct a one-qubit gate and is a prerequisite for the appropriateness of the material to QIP. Figure 5 (top) shows the Rabi oscillations of the electron spin system at a microwave field $B_1=8.9$ G (corresponding to 1 dB attenuation). These oscillations were recorded with an echo-detected transient nutation sequence[17,18] for $\mathbf{B}_0$ along $\mathbf{a}^*$. The pulse sequence is shown in the inset of Fig. 5 (top). Rabi oscillations can be simulated by

$$S(t) = S_0 \cos(\Omega_R t)\exp(-t/T_R), \tag{3}$$

with a Rabi frequency $\Omega_R=\Omega_R^{(e)}=20$ MHz and a decay time $T_R=T_R^{(e)}=45$ ns for the electron spin. Owing to inhomogeneous distribution of the microwave field and to local field fluctuations induced by interactions between neighboring spins,[19] the Rabi oscillation damping time is generally much shorter than the phase memory time that characterizes the decay of the coherence between spin states. The phase memory time can be determined from the echo decay resulting from two-pulse $\pi/2$-τ-π Hahn sequence[17] with interpulse spacing τ as shown in Fig. 5 (bottom). Oscillations in the echo decay are due to nuclear modulations. The exponential decay of the background signal shown by the dashed line in Fig. 5 (bottom) gives the electron phase memory time $T_m^{(e)} \approx 1.1\ \mu s$ at 4 K. Increasing the electron phase memory time would certainly be necessary to reach a good fidelity of the spin-bus operations. This could be achieved by reducing the crystal disorder with thermal annealings and by using lower Ti concentrations (thus reducing the efficiency of the electron spin-spin relaxation), however at the expense of the ENDOR signal-to-noise ratio. The observation of nuclear Rabi oscillations is also a key requirement for the spin-bus concept. Nuclear oscillations were detected by pulsed ENDOR with the sequence depicted in Fig. 6, where the first two microwave $\pi/2$ pulses create an electron spin polarization grating, which is modulated by the radio-frequency pulse of increasing duration t at a selected nuclear frequency. The last microwave $\pi/2$ pulse detects the modulated electron spin polarization via a stimulated echo. Figure 6 shows nuclear Rabi oscillations at 8 K at the nuclear frequency 20.2 MHz indicated by the full arrow on the pulsed ENDOR spectrum (inset in Fig. 6), corresponding to a $m_q=0$, $m_S=-1/2$ nuclear transition of ^{69}Ga(4). The definition of m_q is given in Fig. 2. This signal was obtained with $\mathbf{B}_0$ in the $(\mathbf{c},\mathbf{a}^*)$ plane at 45° from **c** and after subtraction of an off-resonance background signal recorded at the frequency shown by the dotted arrow on the ENDOR spectrum (Fig. 6). The simulation of the Rabi oscillations with Eq. (3) gives the nuclear Rabi frequency $\Omega_R=\Omega_R^{(n)}=44$ kHz and the nuclear decay time $T_R=T_R^{(n)}=12\ \mu s$ for the probed nuclear transition. Again, this value is a lower bound for the nuclear phase memory time $T_m^{(n)}$. An upper bound can be obtained from the fact that in the case of strongly coupled electron-nucleus systems

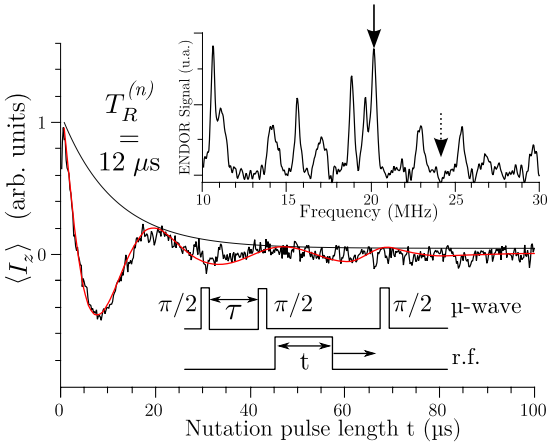

FIG. 6. (Color online) Experimental (black line) and calculated (red line) nuclear Rabi oscillations at 8 K for $\mathbf{B}_0 \perp \mathbf{b}$ and $(\mathbf{c},\mathbf{B}_0)=45°$, for the transition ^{69}Ga(4), $m_q=0$, $m_s=-1/2$ (corresponding to the full line arrow on the ENDOR spectrum), recorded with $\tau=174$ ns, 8 μs delay time between microwave and rf pulses and a microwave pulse length 40 ns. The decay of the oscillation according to Eq. (3) is also represented. The pulse sequence and the corresponding ENDOR spectrum are represented in the inset. The dotted arrow on the ENDOR spectrum is the off-resonance position used for the signal treatment.

($A \gg 1/T_1^{(e)}$, with $T_1^{(e)}$ the electron spin-lattice relaxation time), $T_m^{(n)}$ can reach the maximum value $2T_1^{(e)}$.[20] A measurement of the electron spin-lattice relaxation time by inversion recovery gave $T_1^{(e)} \approx 260 \pm 40$ μs. With $A \approx 35$ MHz for the probed nucleus ^{69}Ga(4) [value deduced from the reported value for ^{71}Ga(4) in Table II], we are clearly in the case of a strongly coupled electron-nucleus system. Thus we can deduce the upper bound $2T_1^{(e)} \approx 520$ μs for $T_m^{(n)}$. A more accurate determination of the value of the nuclear decoherence time as well as a detailed investigation of its dependence on the transition, the orientation and the isotope is necessary. It would probably lead to optimized decoherence times but this is beyond the scope of this paper and will be done in a future work. Nonetheless, the upper bound ≈ 520 μs for the nuclear spin decoherence time in Ga_2O_3:Ti is comparable to the value 400 μs obtained from a Hahn echo decay for the first proposal of spin-bus system (CaF_2:Ce^{3+}).[21]

VI. CONCLUSION AND PERSPECTIVE

This ENDOR study of titanium doped β-Ga_2O_3 showed that the paramagnetic species must be considered as a (Ti^{3+}-e^-) pair rather than a Ti^{3+} ion, whereby a conduction electron is trapped by a Ti^{4+} in an octahedral site. The system exhibits strong hyperfine interactions with neighboring Ga nuclei, owing to an unpaired electron spin density delocalized on at least eight Ga neighbors. This behavior of titanium in β-Ga_2O_3 is unprecedented and contrasts with the behavior of other transition ions, such as Cr^{3+}, Fe^{3+}, or Mn^{2+} in this matrix.[22–24] The EPR spectra of these ions do not exhibit any hyperfine interaction with the neighboring Ga nuclei indicating an unpaired electron wave function highly localized on the central ion. The spin system composed of the unpaired electron on Ti magnetically coupled with neighboring Ga nuclei in β-Ga_2O_3 thus seems to be a possible novel spin-bus system: it exhibits both electron and nuclear quantum oscillations as well as nuclear decoherence times at least as high as in the already demonstrated spin-bus system CaF_2:Ce^{3+}. A possible advantage of β-Ga_2O_3:Ti is the existence of two magnetic isotopes ^{69}Ga and ^{71}Ga with similar abundances and with larger spin multiplicity than for the single isotope ($I=1/2$) ^{19}F in CaF_2:Ce^{3+}, resulting in about 40 resolved hyperfine transitions if only the identified Ga nuclei are considered, and about 100 transitions when including the still unidentified nuclei. This constitutes a quantum register larger than with the nine ^{19}F system in CaF_2:Ce^{3+}. The other potential advantage of β-Ga_2O_3:Ti is the exceptionally strong hyperfine interactions, on the order of several tens of megahertz. This opens up the prospect of using the indirect pseudodipolar interaction between nuclei, which scales as $A^2/g\beta B_0 \approx 0.1-1$ MHz instead of the direct dipolar interaction on the order of 1–10 kHz to implement faster two-qubit gates.

ACKNOWLEDGMENT

The EPR facility at LCMCP-UMR 7574 is supported by Région Ile-de-France.

APPENDIX

The angular patterns of the ENDOR lines for each individual nucleus were simulated by least square and trial and error with the spin Hamiltonian given by Eq. (1),

$$\mathbf{H} = \beta \mathbf{S} \cdot \mathbf{g} \cdot \mathbf{B}_0 + \mathbf{S} \cdot \mathbf{A} \cdot \mathbf{I} + \mathbf{I} \cdot \mathbf{Q} \cdot \mathbf{I} - g_n \beta_n \mathbf{I} \cdot \mathbf{B}_0$$

In the crystal frame corresponding to $(X,Y,Z) \equiv (\mathbf{c}, \mathbf{a}^*, \mathbf{b})$, the interaction tensors have the general expression

$$\mathbf{g} = \begin{pmatrix} g_X & 0 & 0 \\ 0 & g_Y & 0 \\ 0 & 0 & g_Z \end{pmatrix}, \quad \mathbf{A} = \begin{pmatrix} A_{XX} & A_{XY} & A_{XZ} \\ A_{YX} & A_{YY} & A_{YZ} \\ A_{ZX} & A_{ZY} & A_{ZZ} \end{pmatrix},$$

$$\mathbf{Q} = \begin{pmatrix} Q_{XX} & Q_{XY} & Q_{XZ} \\ Q_{YX} & Q_{YY} & Q_{YZ} \\ Q_{ZX} & Q_{ZY} & Q_{ZZ} \end{pmatrix}.$$

We used approximate expressions of the eigenvalues adapted from the second-order perturbation treatment performed by Iwasaki.[12] Let

$$\mathbf{h} = \begin{pmatrix} \cos\theta \cos\varphi \\ \sin\theta \cos\varphi \\ \sin\varphi \end{pmatrix}$$

be the unit vector along the external field $\mathbf{B}_0$, where θ and φ stand for the classical spherical angles in the crystal frame. $\tilde{\mathbf{x}}$ represents the transposed of vector or tensor $\mathbf{x}$. We define the unit vector along the effective Zeeman field seen by the electron as

$$\mathbf{u} = \mathbf{g} \cdot \mathbf{h}/g$$

with

$$g = \sqrt{\tilde{\mathbf{h}} \cdot \tilde{\mathbf{g}} \cdot \mathbf{g} \cdot \mathbf{h}}.$$

We also introduce the tensor

$$\mathbf{K}(m_S) = m_S(\mathbf{A} \,.\, \mathbf{g}/g) - g_n \beta_n B_0 \mathbf{E}$$

with m_S the electron spin quantum number and $\mathbf{E}$ the identity tensor. The unit vector along vector $\mathbf{K}(m_S) \cdot \mathbf{h}$ is defined as

$$\mathbf{k}(m_S) = \mathbf{K}(m_S) \cdot \mathbf{h}/K(m_S)$$

with:

$$K(m_S) = \sqrt{\tilde{\mathbf{h}} \cdot \tilde{\mathbf{K}}(m_S) \cdot \mathbf{K}(m_S) \cdot \mathbf{h}}.$$

The zeroth-, first-, and second-order contributions to the eigenvalue of the spin Hamiltonian are

$$E^{(0)}(m_S, m_I) = g\beta B_0 m_S,$$

$$E^{(1)}(m_s, m_I) = K(m_s) m_I - \frac{1}{2}(\tilde{\mathbf{k}} \cdot \mathbf{Q} \cdot \mathbf{k})[I(I+1) - 3m_I^2],$$

$$E^{(2)}(m_S,m_I) = \frac{1}{2g\beta B_0}\left\{|A_1|^2 m_S m_I^2 - A_2[S(S+1)-m_S^2]m_I + \frac{1}{2}A_3 m_S[I(I+1)-m_I^2]\right\} - \frac{1}{2K(m_S)}\left\{|Q_1|^2 m_I[4I(I+1)-8m_I^2-1] - \frac{1}{4}|Q_2|^2 m_I[2I(I+1)-2m_I^2-1]\right\},$$

with m_I, the nuclear spin quantum number and with

$$|A_1|^2 = \tilde{\mathbf{k}}\cdot\tilde{\mathbf{A}}\cdot\mathbf{A}\cdot\mathbf{k} - (\tilde{\mathbf{k}}\cdot\mathbf{A}\cdot\mathbf{u})^2,$$

$$A_2 = \det[\mathbf{A}(\tilde{\mathbf{u}}\cdot\mathbf{A}^{-1}\cdot\mathbf{k})],$$

$$A_3 = \mathrm{Tr}(\tilde{\mathbf{A}}\cdot\mathbf{A}) - \tilde{\mathbf{u}}\cdot\tilde{\mathbf{A}}\cdot\mathbf{A}\cdot\mathbf{u} - \tilde{\mathbf{k}}\cdot\mathbf{A}\cdot\tilde{\mathbf{A}}\cdot\mathbf{k} + (\tilde{\mathbf{k}}\cdot\mathbf{A}\cdot\mathbf{u})^2,$$

$$|Q_1|^2 = \tilde{\mathbf{k}}\cdot\mathbf{Q}^2\cdot\mathbf{k} - (\tilde{\mathbf{k}}\cdot\mathbf{Q}\cdot\mathbf{k})^2,$$

$$|Q_2|^2 = 2\ \mathrm{Tr}(\mathbf{Q}^2) + (\tilde{\mathbf{k}}\cdot\mathbf{Q}\cdot\mathbf{k})^2 - 4(\tilde{\mathbf{k}}\cdot\mathbf{Q}^2\cdot\mathbf{k}).$$

*laurent-binet@chimie-paristech.fr

[1] W. Warren, N. Gershenfeld, and I. Chuang, Science **277**, 1688 (1997).
[2] N. Linden and S. Popescu, Phys. Rev. Lett. **87**, 047901 (2001).
[3] A. Heidebrecht, J. Mende, and M. Mehring, Solid State Nucl. Magn. Reson. **29**, 90 (2006).
[4] M. Mehring and J. Mende, Phys. Rev. A **73**, 052303 (2006).
[5] E. Aubay and D. Gourier, J. Phys. Chem. **96**, 5513 (1992).
[6] E. Aubay and D. Gourier, Phys. Rev. B **47**, 15023 (1993).
[7] L. Binet and D. Gourier, J. Phys. Chem. **100**, 17630 (1996).
[8] A. Saurat and R. Revcolevcschi, Rev. Int. Hautes Temp. Refract. **8**, 291 (1971).
[9] D. Schoemaker, Phys. Rev. **174**, 1060 (1968).
[10] J. Spaeth and H. Overhof, *Point Defects in Semiconductors and Insulators* (Springer, Berlin, 2003).
[11] R. Barklie, J. Niklas, and J. Spaeth, J. Phys. C **13**, 1757 (1980).
[12] M. Iwasaki, J. Magn. Reson. **16**, 417 (1974).
[13] A. Raüber and J. Schneider, Phys. Status Solidi B **18**, 125 (1966).
[14] T. Vosegaard, I. P. Byriel, L. Binet, D. Massiot, and H. J. Jakobsen, J. Am. Chem. Soc. **120**, 8184 (1998).
[15] G. Denninger, K. Baldenhofer, R. Gessler, L. Binet, and D. Gourier, J. Magn. Reson. **148**, 248 (2001).
[16] I. Rabi, Phys. Rev. **51**, 652 (1937).
[17] A. Schweiger and G. Jeschke, *Principles of Pulse Electron Paramagnetic Resonance* (Oxford University Press, USA, 2001).
[18] S. Bertaina, S. Gambarelli, A. Tkachuk, I. Kurkin, B. Malkin, A. Stepanov, and B. Barbara, Nat. Nanotechnol. **2**, 39 (2007).
[19] R. N. Shakhmuratov, F. M. Gelardi, and M. Cannas, Phys. Rev. Lett. **79**, 2963 (1997).
[20] J. L. Morton, A. Tyryshkin, R. Brown, S. Shankar, B. Lovett, A. Ardavan, T. Schenkel, E. Haller, J. Ager, and S. A. Lyon, Nature (London) **455**, 1085 (2008).
[21] A. Heidebrecht, J. Mende, and M. Mehring, Fortschr. Phys. **54**, 788 (2006).
[22] R. Büscher and G. Lehmann, Z. Naturforsch. **42a**, 67 (1987).
[23] T. H. Yeom, I. G. Kim, S. H. Lee, S. H. Choh, and Y. M. Yu, J. Appl. Phys. **93**, 3315 (2003).
[24] I. G. Kim, T. H. Yeom, S. H. Lee, Y. M. Yu, H. W. Shin, and S. H. Choh, J. Appl. Phys. **89**, 4470 (2001).